Colloids and Surfaces B: Biointerfaces 255 (2025) 114951

Contents lists available at ScienceDirect

Colloids and Surfaces B: Biointerfaces

journal homepage: www.elsevier.com/locate/colsurfb

Optimized synthesis and characterization of highly reproducible carbon dots for bioimaging applications

D. Manno [a,*], M.M. Orlando [a], A. Gabriele [a], G.G. Carbone [a], A. Buccolieri [a], L. Calcagnile [a], A. Bibi [b], D. De Benedictis [b], G. Capitanio [b], D. De Rasmo [c], A. Signorile [b], G. Giancane [d], A. Serra [a]

[a] CEDAD-Centro di Fisica Applicata Datazione e Diagnostica - Dipartimento di Matematica e Fisica "E. De Giorgi", Università del Salento, via Arnesano, Lecce 73100, Italy
[b] Department of Translational Biomedicine and Neuroscience, University of Bari Aldo Moro, P.zza Giulio Cesare, Bari 70124, Italy
[c] Institute of Biomembranes, Bioenergetics and Molecular Biotechnologies (IBIOM), National Research Council of Italy (CNR), Italy
[d] DISTEBA, Università del Salento, via Monteroni, Lecce 73100, Italy

ARTICLE INFO

Keywords:
Doped carbon dots
Photoluminescence
Optical characterization
Electron microscopy characterization
Cytocompatibility
Bioimaging

ABSTRACT

In this paper, we present the optimization of synthesis parameters to obtain highly stable fluorescent Carbon Dots (CDs). This was achieved through a multidisciplinary approach that combined systematic variation of synthesis conditions with comprehensive characterization techniques. Spectroscopic analyses, including absorbance and fluorescence measurements, along with transmission electron microscopy, confirmed the uniform morphology and distinctive optical emission of the CDs. Additionally, electron energy loss spectroscopy provided valuable insights into their chemical composition, while high-resolution transmission electron microscopy (HRTEM) revealed structural order at the nanometer scale. Among the synthesized CDs, those exhibiting the most promising optical and physicochemical properties were further tested to assess their cellular imaging potential, cytocompatibility, and non-toxicity. The data showed that CDs were cytocompatible and can permeate the cell membrane localizing in the cells. Notably, these CDs showed the ability to targeting mitochondria, underscoring their potential for analyses of mitochondrial structure and function in different physiological and pathological conditions.

1. Introduction

Fluorescent carbon dots (CDs) have emerged as a highly promising class of nanomaterials with significant potential for bio-imaging applications [1,2]. These nanoparticles, typically smaller than 10 nanometers in size, are distinguished by their remarkable optical properties, including bright fluorescence, strong photostability, and tunable emission wavelengths [3,4]. Combined with their high biocompatibility and low toxicity, CDs present an attractive alternative to conventional fluorescent markers, such as organic dyes and semiconductor quantum dots [5,6].

CDs are classified as zero-dimensional carbon-based nanomaterials with diverse compositions and structures. They generally feature a central carbon core, which may be either graphitic or amorphous in nature, and are coated with various functional groups, including hydroxyl, carboxyl, and amino groups [7,8]. This surface functionalization plays a crucial role in determining the solubility, stability, and biocompatibility of CDs, directly influencing their overall performance and applications [9].

Carbon dot synthesis can be broadly categorized into two main approaches: top-down and bottom-up methods. The top-down approach involves breaking down larger carbon materials like graphite, carbon nanotubes, or graphene into smaller components. Techniques such as laser ablation, arc discharge, or electrochemical exfoliation are typically used for this purpose [10,11]. However, these methods often require extreme conditions and may introduce unwanted impurities [12]. While effective in generating highly crystalline CDs, these methods tend to be complex and time-consuming [13]. On the other hand, bottom-up methods focus on building CDs from smaller organic precursors via controlled carbonization processes. Common precursors, such as sugars, citric acid, and amino acids, undergo carbonization under specific conditions [14,15]. Techniques like hydrothermal or solvothermal

* Corresponding author.
E-mail address: daniela.manno@unisalento.it (D. Manno).

https://doi.org/10.1016/j.colsurfb.2025.114951
Received 15 May 2025; Received in revised form 1 July 2025; Accepted 11 July 2025
Available online 17 July 2025

carbonization, microwave-assisted synthesis, and template-guided synthesis fall under this category [16]. These methods offer better control over the size, shape, and surface characteristics of CDs, making large-scale production more feasible [17].

One of the most notable features of CDs is their strong fluorescence, which can be attributed to several mechanisms, including:

• Quantum confinement effect: In smaller CDs, the restriction of electron and hole movement within the carbon core leads to energy level quantization, producing light emission [18].

• Surface state emission: Surface defects such as dangling bonds or localized electronic states can serve as radiative recombination centers, enhancing fluorescence [19].

• Molecular fluorophore emission: Fluorescence may also arise from fluorescent molecules incorporated within the carbon matrix [20].

The fluorescence properties of CDs are influenced by factors like size, morphology, surface modifications, and the incorporation of heteroatoms (such as nitrogen, sulfur, and phosphorus) [4,6]. These elements can modify the bandgap, which in turn affects the absorption and emission spectra. By optimizing synthesis conditions, the emission wavelengths of CDs can be fine-tuned to span from ultraviolet to near-infrared regions [8].

The distinctive properties of CDs make them highly promising for bio-imaging applications. They can easily be internalized by a variety of cell types, allowing for the visualization of cellular structures and dynamics [12]. CDs have been employed to label specific organelles, such as mitochondria, lysosomes, and the nucleus, providing valuable insights into cellular processes [14]. Due to their excellent biocompatibility and low toxicity, CDs are also potential candidates for in vivo imaging, enabling the tracking of biological events like tumor growth, drug delivery, and immune responses [17]. The ability to synthesize CDs with different emission wavelengths also facilitates multiplexed imaging, allowing for the simultaneous visualization of multiple biological targets [9]. This capability is especially useful for studying complex biological interactions and disease mechanisms [16].

Despite these advantages, there are challenges to be addressed before CDs can be widely adopted for bio-imaging applications:

• Standardizing synthesis and characterization: Current methods for CDs synthesis often result in inconsistent properties across different batches. Establishing standardized protocols and reliable characterization methods is essential to ensure reproducibility and high-quality imaging agents [11].

• Improving fluorescence quantum yield: While progress has been made in enhancing the fluorescence quantum yield of CDs, further improvements are needed to optimize their performance for imaging applications [7].

• Evaluating long-term safety: While CDs are generally considered biocompatible, comprehensive studies on their long-term toxicity are necessary to assess potential risks in clinical applications [10].

This work aims to address these critical challenges to enable the broader use of CDs in diagnostic imaging for both prognostic and therapeutic purposes. In this study, carbon dots were synthesized using citric acid and urea as precursors, with the goal of optimizing synthesis parameters to ensure maximum reproducibility. We selected citric acid as the carbon source and urea as the nitrogen source for the hydrothermal synthesis of CDs. Citric acid is a naturally occurring, biodegradable compound with low toxicity, making it an ideal carbon precursor. Urea, similarly, is a non-toxic, water-soluble compound widely used in agricultural and biochemical applications. It is naturally present in many living organisms, including humans, where it serves several important functions. In the human body, urea is the primary waste product of protein metabolism. By utilizing these benign precursors, we aimed to synthesize fluorescent CDs suitable for biological labeling applications, while minimizing potential cytotoxic effects and environmental hazards. Various parameters such as temperature, reaction time, and precursor ratio were explored to enhance the properties of the obtained materials. The synthesized carbon dots were characterized using UV-Vis spectroscopy to analyze optical properties, Raman spectroscopy to identify structural features and assess disorder, and transmission electron microscopy (TEM and HRTEM) to investigate morphology, size, and distribution. Additionally, advanced compositional analysis techniques, including energy-dispersive X-ray spectroscopy (EDS), electron energy loss spectroscopy (EELS), and energy-filtered transmission electron microscopy (EFTEM), were employed to determine the elemental composition and chemical structure. In addition, the CDs exhibiting the better optical and physicochemical properties were tested to assess their cellular permeability and cytocompatibility.

2. Experimental

2.1. Synthesis

The synthesis process can be briefly summarized as follows: varying concentrations of citric acid and urea were dissolved in distilled water (Table 1), and the prepared solution was heated in a microwave oven at a power of 540 W for 10 min, reaching a local temperature of 300 °C. The total volume of the solution reached 5 ml. By the end of the process, the solution had turned black. It was then diluted in water and subjected to an ultrasonic bath for 15 min until the product was fully homogenized. The total energy density supplied for the synthesis process was 6.48×10^4 joules/cm^3 .

Purification process was then initiated, consisting of a sequence of filtration and repeated centrifugation over time. Finally, the filtered product underwent further purification using 0.2-micron filters. The synthesis parameters are summarized in Table 1.

During the microwave-assisted process, the reaction mixture, citric acid and urea in aqueous solution, is subjected to rapid and intense heating. A temperature range of 180–220 °C is adequate to trigger the dehydration, polymerization, and carbonization of the precursors [21]. . This temperature range is crucial for the formation of carbon dots with desirable optical properties [22]. On the other hand, prolonged microwave irradiation can cause the temperature to rise further. However, excessive heating may lead to over-carbonization, resulting in larger particles or reduced fluorescence [23,24].

2.2. Characterization

Raman spectra were recorded using a Renishaw inVia Raman Microscope equipped with an Ar^+ 514 nm excitation laser under ambient conditions. The laser power was kept below 1 mW to prevent heating effects. The instrument was calibrated using 520 cm^{-1} band of a silicon wafer. Measurements were performed on dried carbon dot samples deposited onto a clean glass substrate. The acquisition time and number of accumulations were 30 s and 10 accumulations to ensure a good signal-to-noise ratio. Spectra were baseline corrected and analyzed using Renishaw Wire software.

The UV-Vis absorption spectra of the colloidal carbon dot solution were obtained using a Cary 5000 Agilent UV-Vis-NIR spectrophotometer in the range of 200–800 nm. The measurements were carried out using a quartz cuvette with a path length of 1 cm. A solution of deionized water was used as a blank for baseline correction. The colloidal carbon dots were prepared at a concentration of 10 mg/ml and sonicated for 10 min

Table 1
Synthesis parameters, specifically the content of citric acid and urea dissolved in distilled water for all obtained samples.

Sample	Urea CH_4N_2O (g)	Citric Acid $C_6H_8O_7$ (g)	$CH_4N_2O/C_6H_8O_7$ ratio	H_2O (g)
#1	0.45	0.75	0.6	3.80
#2	0.60	0.75	0.8	3.65
#3	0.75	0.75	1.0	3.50
#4	0.90	0.75	1.2	3.35

before measurement to ensure uniform dispersion. Static fluorescence spectra were performed on a RF-5301 PC spectrophotometer (Shimadzu). Absolute photoluminescence quantum yield (PLQY) was measured on FLS 920 with an integrating sphere (Edinburgh).

A Jeol JEM-ARM 200 F NEOARM, operated at 200 kV, was used for TEM, HRTEM, STEM, and Electron Energy Loss Spectroscopy (EELS) to correlate morphological and structural features with chemical composition.

To analyze the carbon nanostructure, high-angle annular dark field (HAADF) imaging was performed in STEM mode using an annular dark field detector. This technique involves scanning a finely focused electron beam across the sample while collecting elastically scattered electrons at high angles (>50 mrad). The resulting contrast enhances variations in density and is highly sensitive to atomic number differences. For optimal imaging conditions, the electron probe was set with a 30 mrad convergence semi-angle, and the camera length was adjusted to 2 cm. Image acquisition was followed by contrast enhancement and noise reduction using Digital Micrograph (DM) software.

To correlate morphology with elemental composition, spectral imaging in STEM (SI-STEM) was performed, combining spatial and spectral information through EELS. In this approach, an electron beam was raster-scanned across the sample, acquiring an energy loss spectrum at each position to generate a hyperspectral data cube with two spatial dimensions and one spectral dimension. EELS spectra were recorded with an energy resolution of 0.3 eV over the range of 220–740 eV to capture carbon, nitrogen, and oxygen uptake. A pixel dwell time of 0.2 s was applied to ensure an adequate signal-to-noise ratio, and the collected data were processed using Digital Micrograph (DM) software.

2.3. Cellular test

The mouse cells NIH3T3 (referred to as 3T3), NIH3T3 transformed with K-ras oncogene mutated at codon 12 G-C (referred to as KRAS) and neonatal normal human dermal fibroblasts (referred as to NHDF-neo) were grown in DMEM High Glucose Medium (Euroclone, Italy) supplemented with 10 % (v/v) Fetal Bovine Serum (FBS), 2 mM Glutamine (NHDF-neo) or 4 mM Glutamine (3T3 and KRAS), 1 % (v/v) Penicillin/Streptomycin at 37 °C, **5 %** CO_2. After the cells reached 80 % confluency, they were washed with Dulbecco's Phosphate Buffered Saline (Euroclone Italy), collected by using trypsin-EDTA in PBS (Euroclone Italy), counted by using Neubauer Chamber, and seeded accordingly to proceed for MTT assay and Confocal Microscopy analysis.

For MTT assay 10,000 cells (3T3, KRAS and NHDF-neo) were seeded in 96-well plate. After 24-hours, the medium was aspirated, and the cells were treated for 1 h with 50 μg/ml of CDs in DMEM. The stock concentration of CDs was 5 mg/ml in DMSO. After CDs treatment the medium was aspirated and cells were treated with 0.25 μg/ml MTT, incubated for 2–3 h at 37∘C until the formation of violet crystals of formazan. MTT solution was removed and 100 μl of Isopropanol was added. The crystals were dissolved by resuspension/pipetting. Absorbance was measured using Cytation 5 Imaging Reader instrument / plate reader (BioTek) at 590 nm. The statistical analysis was performed by Student's *t*-test.

The confocal microscopy analysis was performed to verify intracellular permeability/localization of carbon dots. The cells were seeded in sterilized glass cover slip in 6-multi-well plate.

After 24-hours, the medium was aspirated, and the cells were treated for 1 h with different concentrations of CDs (10, 25 and 50 μg/ml) in DMEM. As reported, after 3 times washing with PBS, the cells were incubated, for15 min at 37 ℃, with 0.3 μM Mitotracker Orange–red specific mitochondrial probe.Then, after washing in PBS, the cells were fixed with 4 % Paraformaldehyde for 10 min at 37 ℃, fixed on glass slides and finally visualized under confocal microscope (Leica) using LASX software for CDs confocal microscope analysis, we used Excitation 405 Emission 488–552Excitation wavelength 488; Emission: 498–567. For analysis of Mitotracker we used Excitation wavelength 552; Emission: 566–625.

3. Results

3.1. Electron microscopy characterization

TEM characterizations were conducted to investigate the morphologies of carbon nanoparticles obtained through different growth processes. Fig. 1 (from a to d) provide a comparative overview, highlighting the structural variations among the samples. The nanoparticles of Sample 1 (Fig. 1a) exhibit weak contrast and indistinct boundaries, which can be attributed to their low degree of crystallinity. The lack of sharp edges and uniformity suggests that these particles may be largely amorphous or contain a high level of disorder in their atomic arrangement. Nanoparticles in Sample 2 (Fig. 1b) exhibit poor contrast, which supports the hypothesis that they have low crystallinity, like Sample 1. Upon closer examination, the nanoparticles in Sample 2 appear slightly more uniform compared to those in Sample 1, indicating some improvement in structural organization. However, the observed changes are not sufficient to establish well-defined crystalline domains. The overall morphology remains indistinct, suggesting that the growth process did not achieve complete graphitization, leaving the material in a partially disordered state, as clearly illustrated in the supplementary material. In contrast, Sample 3 (Fig. 1c) exhibits well-defined edges and significantly enhanced contrast in the TEM images, indicative of a higher degree of crystallinity. The improved contrast suggests stronger electron diffraction, typically associated with more ordered carbon structures.

This implies that the synthesis conditions for Sample 3 promoted better structural organization of carbon atoms, potentially resulting in graphitic domains. The presence of these graphitic regions suggests a more advanced crystallization process compared to Samples 1 and 2, possibly due to optimized growth parameters or post-treatment methods that enhanced graphitization.

TEM image of Sample 4 (Fig. 1e) reveals a heterogeneous mixture of nanostructures. Some regions contain well-defined crystalline nanoparticles, while others exhibit amorphous or poorly structured particles. The persistence of these heterogeneous features even after purification indicates that a higher nitrogen concentration does not necessarily enhance the structural characteristics of the nanoparticles. Additionally, the presence of scattered agglomerates in the background suggests residual byproducts or fragmented carbonaceous materials, signifying incomplete structural refinement.

Since Sample 3 exhibited the most favorable structural characteristics among the analyzed samples, we conducted a more in-depth investigation using SI-STEM and HRTEM techniques. Fig. 2 provides SI-STEM correlative morphology and elemental analysis for Sample 3. The HAADF image (panel a) displays intensity variations corresponding to different atomic densities, effectively highlighting the contrast and clearly revealing the presence of carbon dots. The elemental maps, (b) carbon map and (c) nitrogen, further confirm the co-existence of carbon and nitrogen within the sample.

The uniform distribution of nitrogen throughout the carbon matrix, as observed in the elemental maps, suggests successful nitrogen doping. This even dispersion of nitrogen atoms within the carbon framework indicates that the doping process was effective, potentially influencing the electronic properties and stability of the material. Such structural insights are crucial for understanding how nitrogen incorporation modifies the characteristics of carbon nanoparticles, potentially enhancing their functional properties for targeted applications.

Moreover, electron energy loss spectroscopy (EELS) provides complementary evidence of nitrogen incorporation into the sp^2 carbon matrix. As evident from Fig. 3, the presence of distinct π^* (~400 eV) and σ^* (~405 eV) resonances in the nitrogen K-edge confirms covalent embedding of nitrogen as C–N and C═N bonds 25, rather than simple surface adsorption. This feature is evident in EELS core loss related to

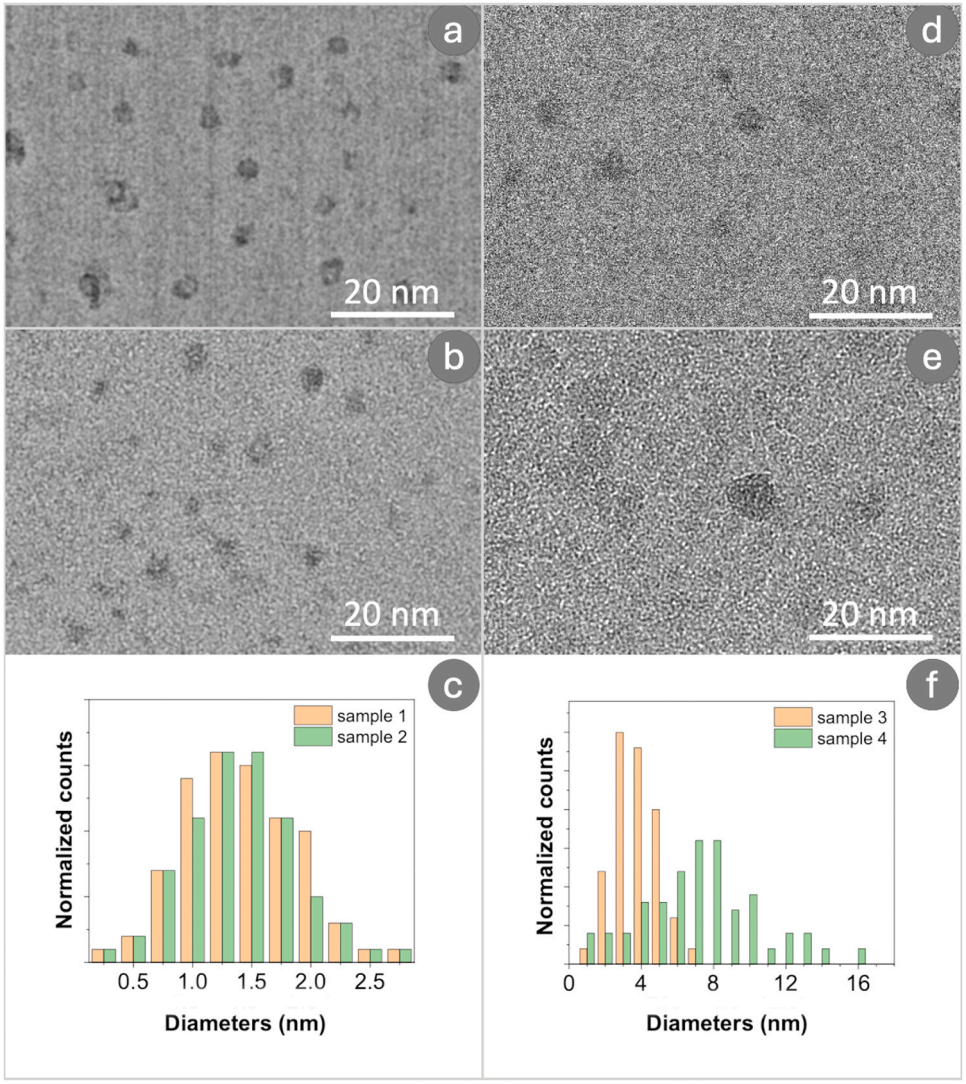

Fig. 1. TEM images of carbon nanoparticles obtained through different growth processes: (a) Sample 1, exhibiting weak contrast and indistinct boundaries, indicative of low crystallinity; (b) Sample 2, showing slightly improved uniformity but still lacking well-defined crystalline domains; (c) Size distribution of CDs in Samples 1 and 2; (d) Sample 3, with well-defined edges and enhanced contrast, suggesting a higher degree of crystallinity and possible graphitic domains; (e) Sample 4, displaying a heterogeneous mixture of crystalline and amorphous nanoparticles; (f) Size distribution of CDs in Samples 3 and 4.

sample 3, is very faint in sample 2 and 4, but result absent in sample 1.

Fig. 4 provides an example of this analysis, presenting HRTEM images (panel a) of the carbon nanoparticles from Sample 3, along with the corresponding Fourier transform (inset). The HRTEM image reveals lattice fringes indicative of a partially ordered structure, suggesting the presence of graphitic domains within the sample. The Fourier transform analysis further supports this observation by displaying distinct intensity distributions along concentric rings. The radii of these rings correspond to the diffraction reflections that are peculiar to graphite, specifically the (002), (100), and (102) planes 26. The presence of the (002) reflection suggests the existence of layered graphitic structures, while the (100) and (102) reflections indicate in-plane order within the carbon matrix.

Figs. 5 present additional HRTEM images of two representative carbon dots found in Sample 3. High-magnification images, shown in panels (c) and (d), provide an enlarged view of these structures, allowing for a more detailed examination of their crystallinity.

The lattice fringes visible in these images confirm the presence of well-ordered carbon structures, with different orientations clearly identifiable, all corresponding to graphite-like nanostructures. The inset of Fig. 5c represents the simulated HRTEM image of a graphite nanoparticle. Notably, in Fig. 5d, a nanoparticle with a distinct single layer of graphene is observed. The inset in this panel presents an HRTEM simulation of a single graphene layer, which closely matches the experimental image. This finding highlights the presence of highly ordered carbon domains within the sample and suggests that the synthesis conditions favored the formation of well-defined graphitic structures with an extent of about 5 nm.

These complementary techniques have been instrumental in gaining a deeper understanding of the structural and compositional properties of carbon dots. The results indicate that nitrogen atoms are incorporated into the cores of CDs, which exhibit a C-graphite hcp structure. However, the nitrogen content is not high enough to significantly alter the crystal structure of graphite itself. Instead, it plays a key role in changing the electronic and chemical properties of the material, contributing to fluorescence activation.

3.2. *Optical properties*

Fig. 6 illustrates the absorption spectra of the synthesized carbon dots, emphasizing the following key features:

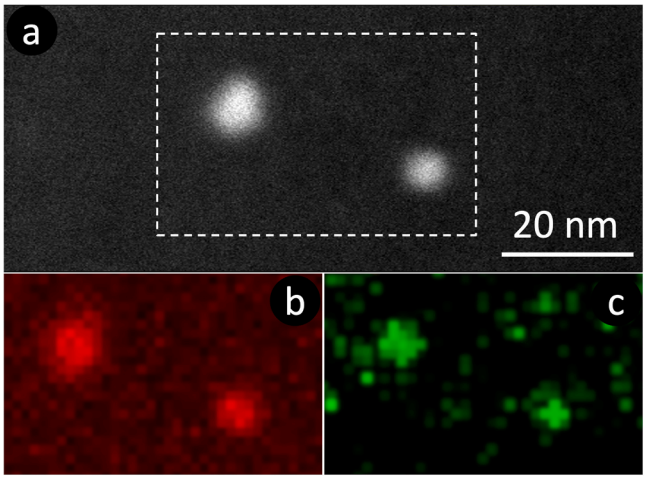

Fig. 2. SI-STEM correlative morphology and elemental analysis of Sample 3: (a) HAADF image showing intensity variations corresponding to different atomic densities, (b) carbon map and (c) nitrogen map show the co-existence of carbon and nitrogen.

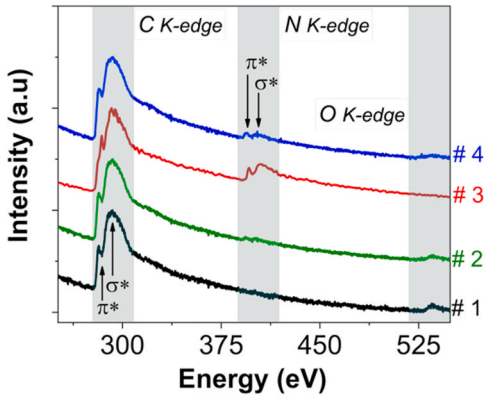

Fig. 3. EELS spectra core loo performed onto the examinate samples.

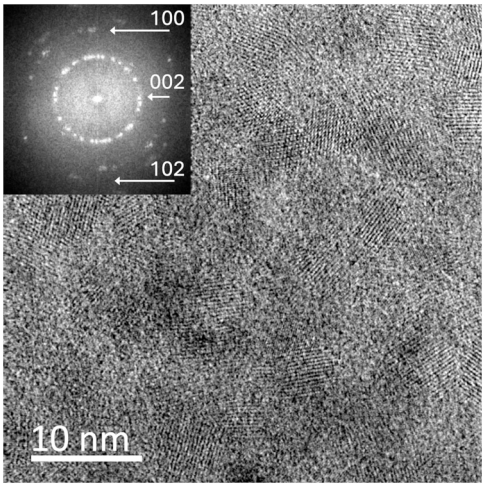

Fig. 4. HRTEM analysis of carbon nanoparticles from Sample 3: (a) HRTEM image displaying lattice fringes indicative of a partially ordered nanostructures; (inset) corresponding Fourier transform showing distinct intensity distributions along concentric rings.

- *π−π* Absorption Bands*: These absorption bands correspond to π−π* electronic transitions within sp^2-conjugated structures commonly found in the carbon dot core. These transitions primarily absorb energy in the ultraviolet or lower-energy visible range, at about 250 nm, significantly influencing the fluorescence behavior of the carbon dots. The specific shape of these bands depends on factors such as core size, defect density, and the degree of conjugation. Additionally, structural modifications, such as the introduction of functional groups or molecular-level interactions, can alter these bands [4,27].
- Charge Transfer Complex (CTC) Band: This band arises from interactions between electron-donor and electron-acceptor groups within the carbon dots. Electron transfer occurs between donor orbitals (e.g., amino or hydroxyl groups) and acceptor orbitals (e.g., carbonyl or carboxyl groups). The position and intensity of the CTC band are influenced by the properties of these groups and the efficiency of charge transfer mechanisms [28].

The absorption spectra further reveal two distinct peaks within the CTC band in addition to the π−π* transition features. The peak near 350 nm corresponds to C−O bonds, while the peak near 400 nm is linked to C−N bonds [29].

The absorption peak at 350 nm is associated with electronic transitions involving oxygen-based functional groups, including alcohols, carboxyls, and carbonyls, introduced during the synthesis process using citric acid. The incorporation of C−O bonds enhances the electronic structure of the carbon dots, increasing surface electron density and improving their UV absorption properties. These functional groups also contribute to surface passivation, leading to modified optical characteristics and enhanced fluorescence [30].

The peak at 400 nm corresponds to C−N bonds, which form when nitrogen-rich precursors like urea are utilized during synthesis. As the urea content increases, the intensity of this peak grows, indicating that nitrogen doping introduces electron donor centers. These centers enhance the conjugation of the π-system and promote lower-energy transitions compared to C−O bonds. Additionally, C−N bonds improve the water solubility, chemical stability, and optical properties of the carbon dots [31]. Interestingly, no significant signals are observed at longer wavelengths associated with n − π* transitions, which typically involve electronic shifts between heteroatoms such as oxygen and nitrogen within functional groups on the carbon dots.

One possible reason for the absence of significant signals at longer wavelengths related to n − π* transitions in carbon dots is their electronic structure and surface chemistry. Typically, n − π* transitions arise from lone pairs on heteroatoms like oxygen and nitrogen interacting with conjugated π systems. However, several factors may suppress or weaken these transitions. Extensive surface passivation with electron-withdrawing groups, such as carboxyl or amide functionalities, can reduce the availability of non-bonding electrons (n) on oxygen and nitrogen, thereby diminishing n − π* transitions [32,33].

Additionally, quantum confinement in CDs influences electronic transitions [34]. As the size of the CDs decreases, their electronic states become more discrete, which can suppress n − π* transitions while enhancing π−π* transitions [35]. Furthermore, the presence of charge transfer complex (CTC) bands in the absorption spectra suggests strong charge transfer interactions between different functional groups [36]. These interactions may lead to lone pair delocalization, thereby reducing the likelihood of n − π* transitions [37].

The absorption spectrum provides further insight, revealing distinct peaks within the CTC band that indicate localized transitions rather than conventional n − π* absorptions. Specifically, the peak observed around 350 nm is attributed to C−O bonds, which are commonly associated with hydroxyl or ether functionalities, while the peak near 400 nm is linked to C−N bonds, potentially arising from amine or amide groups [38].

In addition, the EELS features presented in Fig. 3 provide direct

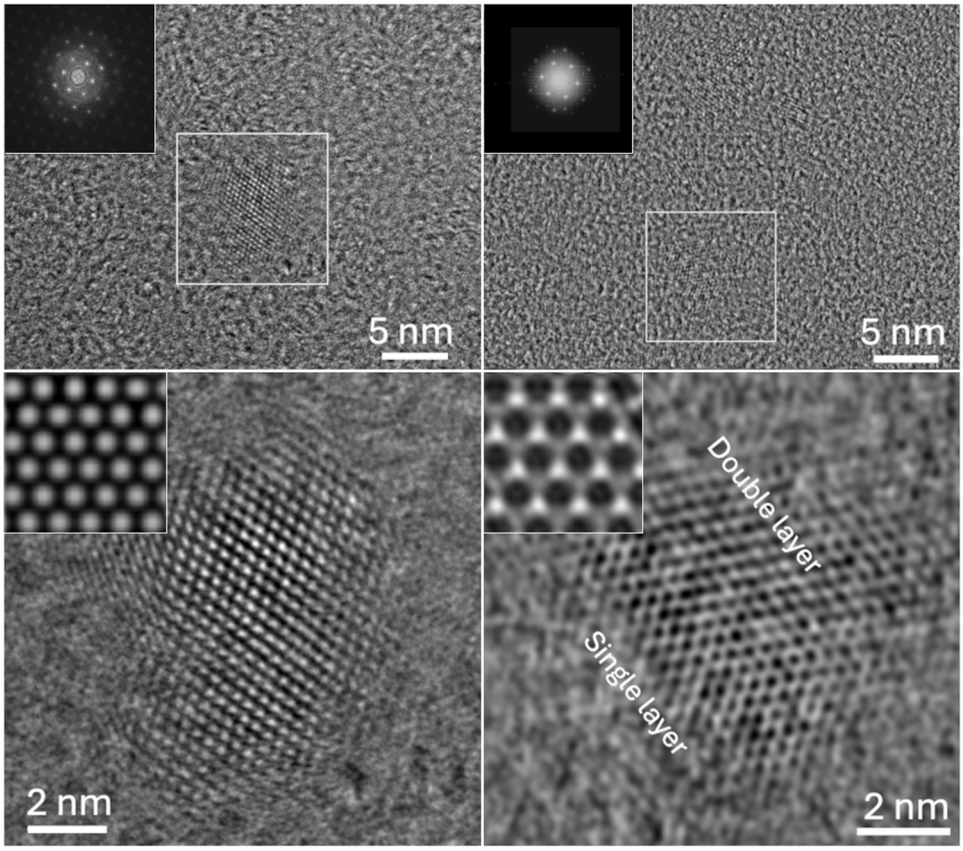

Fig. 5. HRTEM images of representative carbon dots from Sample 3: (a, b) images showing the morphology of two selected CDs, in the inset the related FFT; (c, d) high-magnification images revealing lattice fringes indicative of well-ordered graphite-like nanostructures, in the inset the simulated HRTEM.

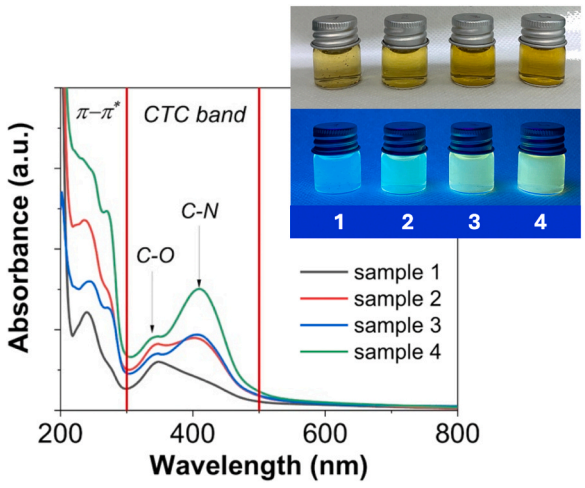

Fig. 6. Absorption spectra of carbon dots feature π−π* transitions in sp^2 domains and a charge transfer complex (CTC) band, influenced by core structure and charge dynamics.

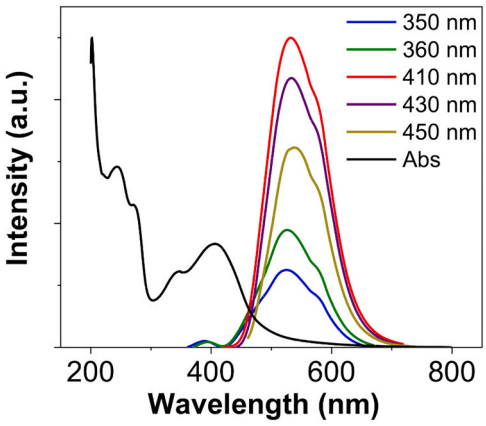

Fig. 7. Absorption spectra of CDs, and emission spectra of sample 3. The CDs excited from 350 to 450 nm wavelength.

spectroscopic evidence of nitrogen incorporation into the carbon lattice, particularly through the formation of C–N and/or C═N bonds. The appearance of both π and σ peaks in the N-edge spectra highlights the strong integration of nitrogen within the sp^2-hybridized carbon framework.

Fig. 7 presents the fluorescence spectra, which display maximum emission when excited at 410 nm, with an emission peak observed around 530 nm.

Across all samples, the maximum emission was consistently observed at an excitation wavelength of 410 nm, indicating that the carbon dots exhibit high sensitivity to excitation at this wavelength [29]. The emission peak near 530 nm falls within the green region of the visible spectrum and is characteristic of carbon dots containing oxygen- and nitrogen-based functional groups (C−O and C−N), which enhance their fluorescence properties [25,29]. The intensity and position of this emission peak are closely tied to the surface chemistry and nitrogen doping of the carbon dots. The π−π* electronic states of the C−O and C−N groups facilitate electronic relaxation and emission processes, with the 530 nm peak indicating effective conjugation and surface passivation [26,27]

To quantify the quantum efficiency of the carbon dots, the

photoluminescence quantum yield (PLQY) at maximum emission (410 nm) was calculated. The PLQY, which represents the efficiency of converting absorbed photons into emitted photons, exhibited distinct behaviors among the four samples analyzed, as shown in Table 2.

An intriguing aspect of the analysis is the relationship between PLQY and the pH of the carbon dot samples, as resumed in table 1 and 2 The fluorescence intensity was observed to reach its maximum at a pH of 4 and remain stable at higher pH values. This observation is consistent with previous studies, which indicate that modifications in the surface structure of terminal carbon atoms—particularly, protonation and deprotonation of functional groups—affect the electronic properties and fluorescence behavior of carbon dots [4,25].

Functional groups such as carboxyl (COOH) and amine (NH_2) groups tend to protonate under acidic conditions, reducing the availability of electronic states for luminescence and thereby decreasing the PLQY. As the pH increases, these groups deprotonate, enhancing the availability of electronic states, improving π-system conjugation, and increasing fluorescence efficiency [27,29].

The observation of maximum PLQY under neutral pH conditions supports findings from earlier studies, which suggest that carbon dots achieve higher fluorescence quantum efficiency near neutral pH. This is attributed to the deprotonation of functional groups, leading to enhanced structural stability and more efficient light emission [26,28]. However, at higher pH levels, the PLQY decreases, likely due to the formation of oxidizing species or structural changes in the carbon dots, which degrade their optical properties and lead to fluorescence quenching [4]. The quantum yield values obtained through the synthesis process reported in this work are higher than those typically reported in the literature for similar hydrothermal syntheses, which generally range from 20 % to 30 %. Yields around 50 % can be achieved by surface passivation processes employing highly toxic compounds such as hydrazine. In cases where barium is used for doping, quantum yields as high as 90 % have been reported [39].

As reported in the supplementary material, the fluorescence properties and quantum efficiency were monitored over a 12-month period, with no appreciable changes observed. The solution was stored at 25 °C in the dark and sonicated for 10 min prior to the measurements.

3.3. Raman spectroscopy

The Raman spectra of the four CDs samples (Fig. 8) exhibit clear D and G peaks in all cases, demonstrating the presence of both disordered and graphitic carbon structures. The D peak, appearing around 1360cm^{-1} , arises from the breathing modes of sp^2-hybridized carbon atoms in six-membered aromatic rings. Its presence is indicative of structural defects, including vacancies, edge states, or the incorporation of heteroatoms (e.g., nitrogen and oxygen) in the carbon lattice. The intensity of the D peak is therefore often used as a marker of the defect density within carbon materials. The G peak, located near 1580 cm^{-1} , corresponds to the in-plane stretching vibrations of sp^2 carbon atoms in graphitic domains [40]. This peak is a hallmark of ordered graphitic structures and provides information about the degree of crystallinity in the material [41].

The positions and relative intensities of these peaks vary systematically with the increasing urea content, indicating a strong influence of nitrogen doping on the structural properties of the CDs [42].

In Sample 1, as highlighted from TEM analysis, the carbon dots are very small and nearly amorphous, leading to a low D peak intensity. As the urea content increases in Samples 2 and 3, the grain size of the CDs grows, and the D peak intensity also increases, reflecting a rise in structural defects associated with the expansion of sp^2 domains and the incorporation of nitrogen. However, in Sample 4, which contains the highest urea concentration, the D peak intensity decreases despite further grain growth and increased crystallinity. This suggests that at high nitrogen doping levels, defect passivation becomes more effective, leading to a reduction in disorder within the structure.

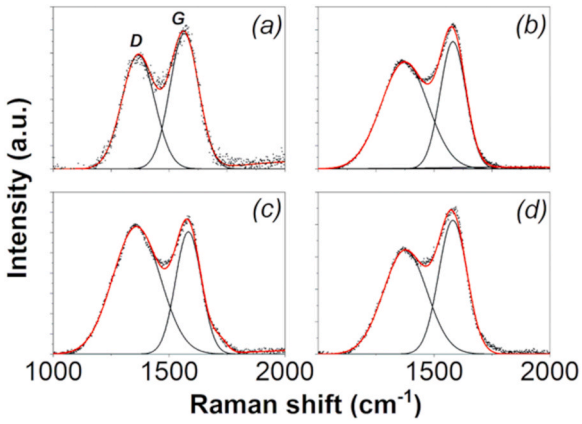

Fig. 8. Raman spectra of CDs obtained through different growth processes: (a) Sample 1, (b) Sample 2, (c) Sample 3, (d) Sample 4.

The G peak, located near 1580 cm^{-1} , becomes more pronounced and slightly sharper with increasing urea content. This observation points to an enhancement in the crystallinity and graphitic character of the CDs as more nitrogen is incorporated. Nitrogen atoms, when doped into the graphitic structure, enhance π-conjugation and stabilize the sp^2 network, leading to an increase in the degree of order [43].

The tabulated data, reported in Table 3 further support the structural evolution of CDs with increasing urea content. In Table 3 are reported the D and G position, the full width at half maximum (FWHM) of D and G peak (Γ_D and Γ_G) and the integral intensity ratio of the D and G peaks (I_D/I_G). The position of the D peak shifts slightly from 1367 cm^{-1} in Sample 1–1371 cm^{-1} in Samples 2 and 4, indicating minor structural modifications due to nitrogen incorporation. Similarly, the G peak shifts from 1579 cm^{-1} in Sample 1–1584 cm^{-1} in Sample 3, suggesting an increase in graphitic order as nitrogen stabilizes the sp^2 network.

Γ_D increases significantly from 165 cm^{-1} in Sample 1–240 cm^{-1} in Sample 3, highlighting an increase in structural disorder due to nitrogen doping. However, in Sample 4, Γ_D decreases to 221 cm^{-1} , supporting the idea that excessive nitrogen content leads to defect passivation and a reduction in disorder. A similar trend is observed for the G peak width (Γ_G), which first decreases from 145 cm^{-1} (Sample 1) to 130 cm^{-1} (Samples 2 and 3), indicating improved crystallinity, but then slightly increases to 143 cm^{-1} in Sample 4, suggesting a limit to the order enhancement.

The relative integral intensity ratio of the D and G peaks (I_D/I_G) is a key parameter for evaluating the balance between disordered and ordered structures in carbon-based systems. A lower (I_D/I_G) ratio suggests

Table 2
efficiency of converting absorbed photons into emitted photons (PLQY).

Sample	CDs solution pH	PLQY (410 nm)
#1	3.30 ± 0.05	**34 %**
#2	3.80 ± 0.05	**57 %**
#3	4.70 ± 0.05	**58 %**
#4	5.30 ± 0.05	**55 %**

Table 3
Parameters determined by Raman analysis. For each analyzed sample are given D and G position, Γ_D, Γ_G and Raman peak intensity ratio I_D/I_G.

Sample	D position (cm^{-1})	G position (cm^{-1})	Γ_D (cm^{-1})	Γ_G (cm^{-1})	I_D/I_G
# 1	**1367**	**1579**	**165**	**145**	**0.96**
# 2	**1371**	**1581**	**238**	**130**	**1.52**
# 3	**1369**	**1584**	**240**	**130**	**1.87**
# 4	**1371**	**1581**	**221**	**143**	**1.20**

greater crystalline order, while a higher ratio indicates a higher density of defects and disordered regions. In Sample 1, the (I_D/I_G) ratio is initially low due to the small size and quasi-amorphous nature of the CDs. In Samples 2 and 3, the ratio increases as the grain size grows and structural defects become more pronounced. However, in Sample 4, the (I_D/I_G) ratio decreases again, indicating a reduction in defect density despite continued grain growth, likely due to nitrogen passivation effects.

Nitrogen doping reduces structural defects by passivating dangling bonds and edge states within the carbon lattice. In addition, the incorporation of nitrogen facilitates the growth of sp^2-domains, promoting a more ordered graphitic structure [44].

The systematic improvement in crystalline order with increasing urea content highlights the crucial role of nitrogen doping in the structural evolution of CDs. Nitrogen atoms preferentially substitute carbon atoms in the lattice, contributing to the stabilization of graphitic domains. Additionally, nitrogen doping increases the overall electronic density in the carbon network, enhancing π-conjugation and facilitating the formation of larger and more ordered sp^2 clusters.

The observed trends in the Raman spectra align with changes in the optical properties of the CDs reported in earlier sections. The enhanced crystalline order and reduced defect density in nitrogen-rich CDs contribute to improved fluorescence properties, as the well-defined sp^2 domains and nitrogen dopants act as efficient radiative recombination centers [45]. The systematic increase in crystallinity also results in better-defined absorption and emission features, as observed in UV-Vis and photoluminescence spectra. However, it is important to note that during the hydrothermal synthesis of carbon dots, the addition of urea does not lead to a continuous improvement in fluorescence performance. Optical measurements reveal a saturation effect, suggesting that while nitrogen doping initially enhances fluorescence by improving crystallinity and passivation, excessive urea content does not provide further benefits to the optical properties of the CDs.

3.4. Cellular test

Fundamental for the application of fluorescent nanostructures is the verification of the cellular permeability of carbon dots.To study cellular permeability, different cell lines were used: 3T3

KRAS and NHDF-neo. All cells were incubated for 1 h in the same DMEM (Dulbecco's Modified Eagle Medium) culture medium, in which various concentrations of CDs (10 μg/ml, 25 μg/ml, and 50 μg/ml) were dispersed.

As show in the Figs. 9 and 10, laser scanning confocal microscope analysis (LSCM) (conducted with excitation at 405 and recording the emission signal in the spectral range of 488–552 nm) showed that the CDs were able to permeate the cells in dose-dependent manner.

Next, the cytocompatibility of the CDs was evaluated using the MTT assay, a colorimetric test that measures the metabolic activity of cells by revealing the reduction of tetrazolium salts. The color development is proportional to the metabolic activity. The MTT test was performed using the highest concentration of CDs used to obtain the images showed in Fig. 10 - panel A. In addition, fluorescence intensity in 3T3, KRAS, and NHDF-neo cells treated with increasing concentrations of CDs was quantified using ImageJ. The results are presented in the bar graph in Panel B of Fig. 10 as mean values ± SEM (n = 10 fields/images per condition). Statistical significance was assessed using Student's *t*-test; *p < 0.05, **p < 0.01.

The biomedical applications of CDs in areas such as bioimaging, biosensing to drug delivery, make the evaluation of the intracellular localization of these nanostructures very interesting. For this reason, we conducted preliminary experiments to analyze the possible localization of CDs in the mitochondria, cellular organelles, that play a critical role in several physiopathological/pathological conditions such as aging, neurodegeneration, metabolic disease and cancer [46,47].

The NHDF-neo cells were incubated with 10μg/ml of CDs and then

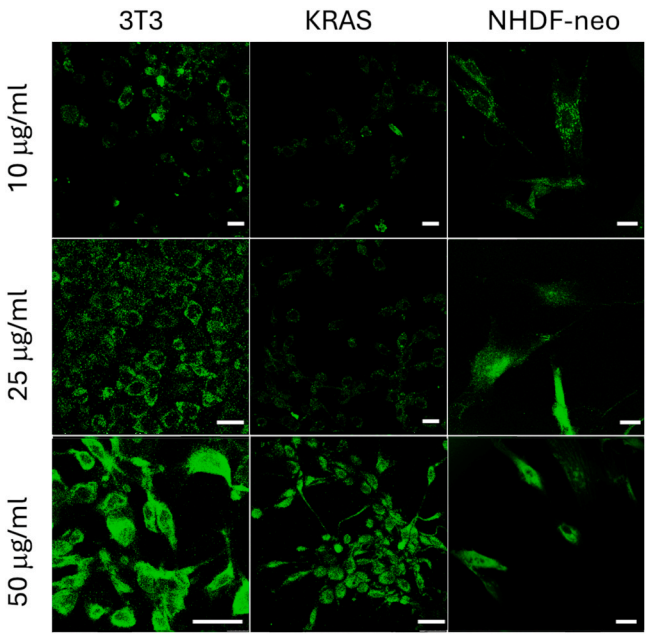

Fig. 9. Representative confocal microscopy images of 3T3, KRAS, and NHDF-neo cells treated with CDs at varying concentrations. Images are obtained by an excitation wavelength Excitation 405 Emission 488–552. The markers in all pictures correspond to 25 mm.

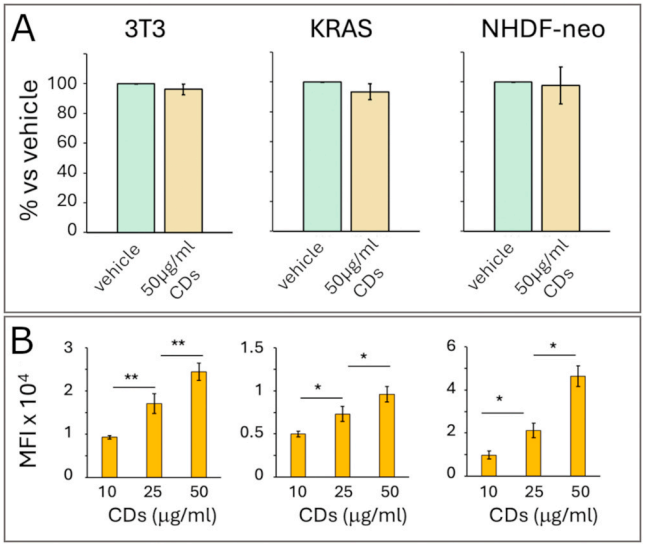

Fig. 10. Panel A: MTT assay results showing cell viability after 1-hour treatment with 50 μg/ml CDs. Panel B: Quantification of fluorescence intensity in 3T3, KRAS, and NHDF-neo cells treated with increasing concentrations of CDs.

with 0.3 μM Mitotracker Orange–red (M7510) for 15 min at 37 °C, *a* selective permeant mitochondrial marker. As evident from Fig. 11, LSCM analysis conducted for visualization of fluorescence of CDs and for mitotraker confirmed the mitochondria-targeting ability of CDs.

The analysis demonstrates the successful permeation of carbon dots in various cell lines, confirming their potential as fluorescent markers for cellular imaging applications. The use of confocal microscopy to observe the cellular uptake of CDs provides a clear visualization of their intracellular localization, highlighting their ability to traverse the cellular membrane across different types of cells: fibroblasts (3T3), transformed fibroblasts (KRAS) and human fibroblasts (NHDF-neo). In addition, a detailed colocalization analysis between CDs and the mitochondria-

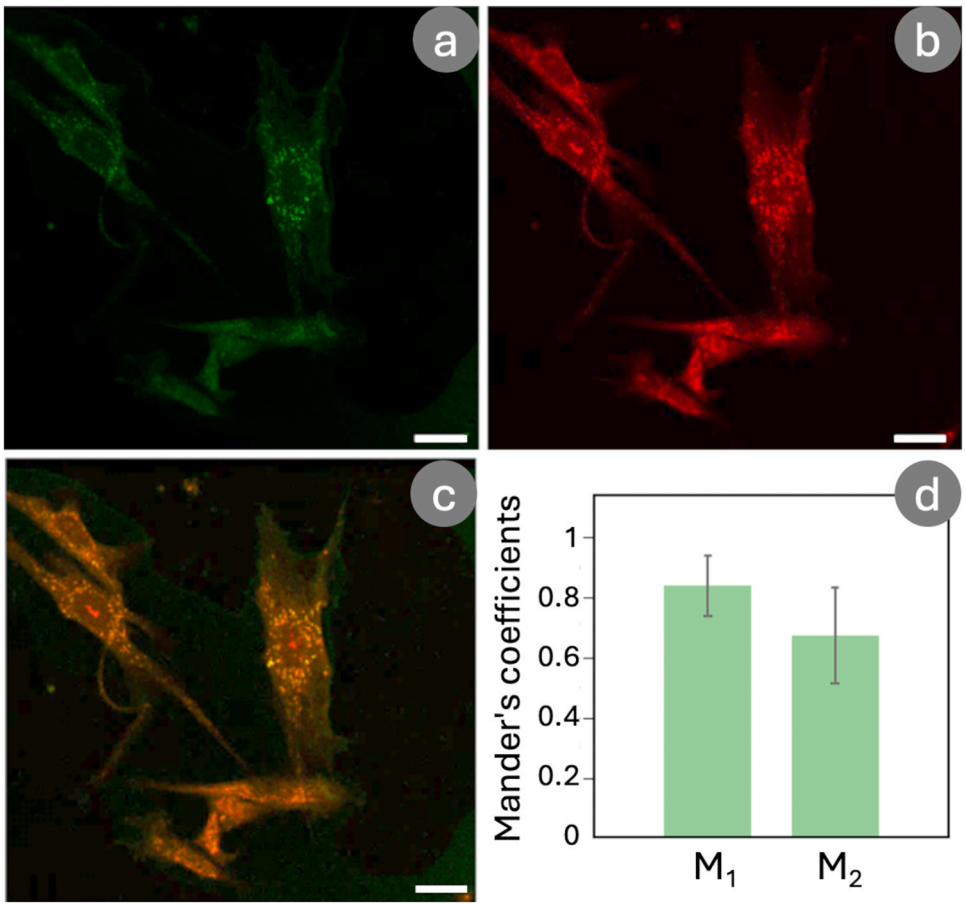

Fig. 11. Confocal microscopy images of NHDF-neo cells treated with 10 μg/ml CDs for 1 h (a), followed by staining with 0.3 μM Mitotracker Orange–Red (b). Picture (c) displays the merged image combining the signals shown in (a) and (b). Cells were fixed and visualized using a Leica confocal microscope. Excitation/emission wavelengths: CDs (405/488–552), Mitotracker (552/566–625 nm). The markers in all pictures correspond to 25 mm. Mander's coefficients quantifications (d).

specific probe Mitotracker Orange–Red demonstrated a substantial spatial overlap, with approximately 80 % of the CD-associated signal colocalizing with mitochondria (Fig. 11d). This was quantitatively assessed by calculating Mander's coefficient M1 using the JACoP plugin in ImageJ, applying an automated thresholding method to ensure objective and reproducible quantification.

This result suggests the application of CDs for specific analyses of mitochondrial structure and function. This broad applicability suggests that CDs could be versatile tools in bioimaging and diagnostic fields.

The cytocompatibility of CDs, assessed through the MTT assay, indicates that CDs do not adversely affect the metabolic activity of the cells at the concentrations tested (50 μg/ml). This is a crucial finding, as it underscores the potential of CDs to be used safely in living cells without inducing cytotoxic effects, which is often a significant concern with nanomaterials.

Future studies could extend this work by exploring the long-term effects of CDs on cellular health and their behavior in different biological environments.

4. Conclusions

In this study, we analysed the structural and optical properties of nitrogen-doped carbon dots synthesized under varying conditions, evaluated their effectiveness as fluorescent biomarkers, and confirmed their excellent biocompatibility.

Structural analysis confirmed that optimized nitrogen doping enhances crystallinity and promotes well-defined graphitic domains, as observed in Sample 3. TEM, HRTEM, and SI-STEM analyses validated the successful incorporation of nitrogen into the carbon lattice, influencing the electronic properties and overall structural integrity of the CDs. However, excessive nitrogen doping led to the formation of heterogeneous structures, highlighting the importance of controlled synthesis.

Optical characterization demonstrated that nitrogen doping significantly improved fluorescence efficiency, with PLQY measurements confirming enhanced optical performance up to a saturation point. The absorption and emission spectra reflected strong π–π* transitions and charge transfer complex bands, further emphasizing the impact of nitrogen incorporation on electronic transitions.

Biological assessments showed that CDs permeate cells efficiently without inducing cytotoxic effects. Confocal microscopy and MTT assays confirmed their biocompatibility across multiple cell lines, reinforcing their suitability for bioimaging applications. The analysis of confocal microscopy merge images, obtained by treating the NHDF-neo with CDs and specific mitochondrial probe, showed a clear colocalization, suggesting that CDs can localize in the mitochondria.

Overall, our findings underscore the pivotal role of nitrogen doping in tuning the properties of CDs for potential applications in bioimaging and optoelectronics. Future research should explore tailored functionalization strategies to further optimize their stability and performance in complex biological environments, including in vivo models.

CRediT authorship contribution statement

Alessandra Gabriele: Methodology, Investigation. **Antonio Serra:** Writing – review & editing, Writing – original draft, Project

administration, Methodology, Investigation, Data curation, Conceptualization. **Mattia M Orlando:** Investigation, Data curation. **Alessandro Buccolieri:** Writing – original draft, Investigation. **Giorgio G Carbone:** Methodology, Data curation. **Lucio Calcagnile:** Visualization, Supervision, Conceptualization. **Daniela De Benedictis:** Investigation, Data curation. **Aasia Bibi:** Investigation, Formal analysis. **Domenico De Rasmo:** Validation, Methodology. **Giuseppe Capitanio:** Methodology, Investigation, Formal analysis. **Gabriele Giancane:** Investigation, Data curation. **Daniela Manno:** Writing – review & editing, Writing – original draft, Software, Methodology, Investigation, Formal analysis, Data curation. **Anna Signorile:** Writing – original draft, Methodology, Investigation, Data curation, Conceptualization.

Declaration of Competing Interest

The authors declare that they have no known competing financial interests or personal relationships that could have appeared to influence the work reported in this paper.

Acknowledgments

This work was carried out within the framework of the PRIN-PNRR 2022 CAR-BIO-MED project CUP F61B23000370006 Ministry of University and Research of Italy (MUR-Italy) During the preparation of this article, the authors used ChatGPT to detect possible plagiarism and check for other writing issues. After using this tool, the authors revised and edited the content as needed and take full responsibility for the content of the publication.

Appendix A. Supporting information

Supplementary data associated with this article can be found in the online version at doi:10.1016/j.colsurfb.2025.114951.

Data availability

Data will be made available on request.

References

[1] S.N. Baker, G.A. Baker, Luminescent carbon nanodots: emergent nanolights, Angew. Chem. Int. Ed. 49 (2010) 6726–6744, https://doi.org/10.1002/anie.200906623.
[2] Y.P. Sun, B. Zhou, Y. Lin, W. Wang, K.A.S. Fernando, P. Pathak, M.J. Meziani, B. A. Harruff, X. Wang, H. Wang, P.G. Luo, H. Yang, M.E. Kose, B. Chen, L.M. Veca, S. Y. Xie, Quantum-sized carbon dots for bright and colorful photoluminescence, J. Am. Chem. Soc. 128 (2006) 7756–7757, https://doi.org/10.1021/ja062677d.
[3] H. Li, Z. Kang, Y. Liu, S.T. Lee, Carbon nanodots: synthesis, properties and applications, J. Mater. Chem. 22 (2012) 24230–24253, https://doi.org/10.1039/C2JM32517H.
[4] S. Zhu, Y. Song, X. Zhao, J. Shao, J. Zhang, B. Yang, The photoluminescence mechanism in carbon dots (graphene quantum dots, carbon nanodots): current state and future perspective, Nano Res. 8 (2015) 355–381, https://doi.org/10.1007/s12274-014-0644-3.
[5] S.Y. Lim, W. Shen, Z. Gao, Carbon quantum dots and their applications, Chem. Soc. Rev. 44 (2015) 362–381, https://doi.org/10.1039/C4CS00269E.
[6] Y. Wang, A. Hu, Carbon quantum dots: synthesis, properties and applications, J. Mater. Chem. C. 2 (2014) 6921–6939, https://doi.org/10.1039/C4TC00988F.
[7] Y. Dong, H. Pang, H.B. Yang, C. Guo, J. Shao, Y. Chi, C.M. Li, T. Yu, Carbon-based dots co-doped with nitrogen and sulfur for high quantum yield and excitation-independent emission, Angew. Chem. Int. Ed. 52 (2013) 7800–7804, https://doi.org/10.1002/anie.201301968.
[8] S. Zhu, Q. Meng, Wang, J. Zhang, Y. Song, H. Jin, K. Zhang, H. Sun, H. Wang, B. Yang, Highly photoluminescent carbon dots for multicolor patterning, sensors, and bioimaging, Angew. Chem. Int. Ed. 52 (2013) 3953–3957, https://doi.org/10.1002/anie.201300519.
[9] H. Liu, T. Ye, C. Mao, Fluorescent carbon nanoparticles derived from candle soot, Angew. Chem. Int. Ed. 46 (2007) 6473–6475, https://doi.org/10.1002/anie.200701271.
[10] H. Li, X. He, Z. Kang, H. Huang, Y. Liu, J. Liu, S. Lian, C.H.A. Tsang, X. Yang, S. T. Lee, Water-soluble fluorescent carbon quantum dots and photocatalyst design, Angew. Chem. Int. Ed. 49 (2010) 4430–4434, https://doi.org/10.1002/anie.200906154.
[11] A. Zhao, Z. Chen, C. Zhao, N. Gao, J. Ren, X. Qu, Recent advances in bioapplications of C-dots, Carbon 85 (2015) 309–327, https://doi.org/10.1016/j.carbon.2014.12.045.
[12] F. Wang, Y.H. Chen, C.Y. Liu, D. Ma, White light-emitting devices based on carbon dots' electroluminescence, Chem. Commun. 47 (2011) 3502–3504, https://doi.org/10.1039/C0CC05391K.
[13] H. Zhu, X. Wang, Y. Li, Z. Wang, F. Yang, X. Yang, Microwave synthesis of fluorescent carbon nanoparticles with electrochemiluminescence properties, Chem. Commun. (34) (2009) 5118–5120, https://doi.org/10.1039/B907612C.
[14] R. Liu, D. Wu, S. Liu, K. Koynov, W. Knoll, Q. Li, An aqueous route to multicolor photoluminescent carbon dots using silica spheres as carriers, Angew. Chem. Int. Ed. 48 (2009) 4598–4601, https://doi.org/10.1002/anie.200900652.
[15] Z. Zhang, J. Zhang, N. Chen, L. Qu, Graphene quantum dots: an emerging material for energy-related applications and beyond, Energy Environ. Sci. 5 (2012) 8869–8890, https://doi.org/10.1039/C2EE22982J.
[16] X. Xu, R. Ray, Y. Gu, H.J. Ploehn, L. Gearheart, K. Raker, W.A. Scrivens, Electrophoretic analysis and purification of fluorescent single-walled carbon nanotube fragments, J. Am. Chem. Soc. 126 (2004) 12736–12737, https://doi.org/10.1021/ja040082h.
[17] Y. Liu, N. Xiao, J. Gong, H. Wang, X. Shi, W. Gu, L. Ye, One-step microwave-assisted polyol synthesis of green luminescent carbon dots as optical nanoprobes, Carbon 68 (2014) 258–264, https://doi.org/10.1016/j.carbon.2013.10.086.
[18] Q. Wang, S. Zhang, T. Wang, P. Li, Q. Zhou, Z. Zhang, Fluorescent carbon dots as an efficient siRNA nanocarrier for its interference therapy in gastric cancer cells, J. Nanobiotechnol. 12 (2014) 58, https://doi.org/10.1186/s12951-014-0058-0.
[19] Y. Dong, J. Shao, C. Chen, H. Li, R. Wang, Y. Chi, X. Lin, G. Chen, Blue luminescent graphene quantum dots and graphene oxide prepared by tuning the carbonization degree of citric acid, Carbon 50 (2012) 4738–4743, https://doi.org/10.1016/j.carbon.2012.06.002.
[20] S. Zhu, J. Zhang, C. Qiao, S. Tang, Y. Li, W. Yuan, B. Li, L. Tian, F. Liu, R. Hu, H. Gao, H. Wei, H. Zhang, H. Sun, B. Yang, Surface chemistry routes to modulate the photoluminescence of graphene quantum dots: from fluorescence mechanism to up-conversion bioimaging applications, Adv. Funct. Mater. 22 (2012) 4732–4740, https://doi.org/10.1002/adfm.201201499.
[21] Z. Zhao, J. Zhang, Y. Chen, Microwave-assisted synthesis of carbon dots: a review of process, mechanism, and applications, Nano Res. 11 (2018) 3031–3043, https://doi.org/10.1016/j.carpta.2022.100218.
[22] H. Li, Z. Kang, Y. Liu, S.T. Lee, Carbon nanodots: Synthesis, properties, and applications, J. Mater. Chem. 22 (2012) 24230–24253, https://doi.org/10.1039/C2JM34690G.
[23] A. Khayal, V. Dawane, M.A. Amin, V. Tirth, V.K. Yadav, A. Algahtani, S.H. Khan, S. Islam, K.K. Yadav, B.-H. Jeon, Advances in the methods for the synthesis of carbon dots and their emerging applications, Polymers 13 (2021) 3190, https://doi.org/10.3390/polym13183190.
[24] Woosung Kwon, Sungan Do, Ji-Hee Kim, Mun Seok Jeong, Shi-Woo Rhee, Control of photoluminescence of carbon nanodots via surface functionalization using para-substituted anilines, Sci. Rep. 5 (2015) 12604, https://doi.org/10.1038/srep12604.
[25] X. Yu, T. Fan, W. Chen, Z. Chen, Y. Dong, H. Fan, W. Fang, X. Yi, Self-hybridized coralloid graphitic carbon nitride deriving from deep eutectic solvent as effective visible light photocatalysts, Carbon 144 (2019) 649–658, https://doi.org/10.1016/j.carbon.2018.12.104.
[26] M. Rossi, D. Manno, S. Orlanducci, A. Serra, M.L. Terranova, Electron diffraction analysis of carbon-based nanomaterials, Encycl. Nanosci. Nanotechnol. 13 (2011) 375–425. https://www.ingentaconnect.com/contentone/asp/enn2/2011/00000013/00000001/art00015.
[27] K. Hola, Y. Zhang, Y. Wang, E.P. Giannelis, R. Zboril, A.L. Rogach, Carbon dots—Emerging light emitters for bioimaging, cancer therapy, and optoelectronics, Nano Today 9 (2014) 590–603, https://doi.org/10.1016/j.nantod.2014.09.004.
[28] A.B. Bourlinos, A. Stassinopoulos, D. Anglos, R. Zboril, M. Karakassides, E. P. Giannelis, Surface functionalized carbogenic quantum dots, Small 4 (2008) 455–458, https://doi.org/10.1002/smll.200700578.
[29] S.Y. Lim, W. Shen, Z. Gao, Carbon quantum dots and their applications, Chem. Soc. Rev. 44 (2015) 362–381, https://doi.org/10.1039/C4CS00269E.
[30] Y. Dong, R. Wang, H. Li, J. Shao, Y. Chi, G. Chen, Polyamine-functionalized carbon quantum dots and their use in sensing glucose, Anal. Chem. 85 (2013) 7003–7009, https://doi.org/10.1016/j.carbon.2012.02.046.
[31] Y. Song, S. Zhu, S. Zhang, Y. Fu, L. Wang, X. Zhao, B. Yang, Investigation from chemical structure to photoluminescent mechanism: a type of carbon dots from the pyrolysis of citric acid and an amine, J. Mater. Chem. C. 3 (2015) 5976–5984, https://doi.org/10.1039/C5TC00813A.
[32] X. Zhao, Y. Li, Z. Wang, Surface passivation effects on the electronic transitions of carbon dots, Carbon 195 (2022) 512–520, https://doi.org/10.21203/rs.3.rs-4021075/v1.
[33] H. Shabbir, E. Csapó, M. Wojnicki, Carbon quantum dots: the role of surface functional groups and proposed mechanisms for metal ion sensing, Inorganics 11 (2023) 262, https://doi.org/10.3390/inorganics11060262.
[34] A. Bhattacharya, S. Chatterjee, R. Prajapati, T.K. Mukherjee, Size-dependent penetration of carbon dots inside the ferritin nanocages: evidence for the quantum confinement effect in carbon dots, Phys. Chem. Chem. Phys. 17 (2015) 12833–12840, https://doi.org/10.1039/C5CP00543D.
[35] R. Ghasemi, A. Arab, S. Manouchehri, Tuning the dual-color fluorescence emission of nitrogen-doped carbon dots by changing nitrogen doping amounts, Russ. J. Gen. Chem. 93 (2023) 2161–2170, https://doi.org/10.1134/S1070363223080248.

[36] M.L. Liu, B.Bin Chen, C.Mei Li, C.Zhi Huang, Carbon dots: synthesis, formation mechanism, fluorescence origin and sensing applications, Green Chem. 21 (2019) 449–471, https://doi.org/10.1039/C8GC02736F.
[37] Ö.K. Koç, A. Üzer, R. Apak, Heteroatom-doped carbon quantum dots and polymer composite as dual-mode nanoprobe for fluorometric and colorimetric determination of picric acid, ACS Appl. Mater. Interfaces 15 (2023) 42066–42079, https://doi.org/10.1021/acsami.3c07938.
[38] K. Patel, D. Sharma, P. Roy, Spectroscopic analysis of C−O and C−N bonding in functionalized carbon dots, Spectrochim. Acta A Mol. Biomol. Spectrosc. 252 (2021) 119493, https://doi.org/10.1016/j.saa.2021.119493.
[39] D. Ozyurt, M. Al Kobaisi, R.K. Hocking, B. Fox, Properties, synthesis, and applications of carbon dots: a review, Carbon Trends 12 (2023) 100276, https://doi.org/10.1016/j.cartre.2023.100276.
[40] M.S. Dresselhaus, G. Dresselhaus, R. Saito, A. Jorio, Raman spectroscopy of carbon nanotubes, Phys. Rep. 409 (2005) 47–99, https://doi.org/10.1016/j.physrep.2004.10.006.
[41] A.C. Ferrari, J. Robertson, Interpretation of Raman spectra of disordered and amorphous carbon, Phys. Rev. B 61 (2000) 14095–14107, https://doi.org/10.1103/PhysRevB.61.14095.
[42] X. Li, M. Rui, J. Song, Z. Shen, H. Zeng, Carbon and graphene quantum dots for optoelectronic and energy devices: a review, Adv. Funct. Mater. 25 (2015) 4929–4947, https://doi.org/10.1002/adfm.201501250.
[43] X. Wang, K. Qu, B. Xu, J. Ren, X. Qu, Microwave assisted one-step green synthesis of cell-permeable multicolor photoluminescent carbon dots for pH sensing in living cells, J. Mater. Chem. 20 (2010) 1539–1545, https://doi.org/10.1039/C0JM02963G.
[44] X. Wang, X. Li, L. Zhang, Y. Yoon, P.K. Weber, H. Wang, J. Guo, H. Dai, N-doping of graphene through electrothermal reactions with ammonia, Science 324 (2009) 768–771, https://doi.org/10.1126/science.1170335.
[45] X. Wang, L. Cao, S.T. Yang, F. Lu, M.J. Meziani, L. Tian, K.W. Sun, M.A. Bloodgood, Y.P. Sun, Bandgap-like strong fluorescence in functionalized carbon nanoparticles, Angew. Chem. Int. Ed. 49 (2010) 5310–5314, https://doi.org/10.1002/anie.201000982.
[46] S. Pahal, N. Mainali, M. Balasubramaniam, R.J. Shmookler Reis, S. Ayyadevara, Mitochondria in aging and age-associated diseases, Mitochondrion 82 (2025) 102022, https://doi.org/10.1016/j.mito.2025.102022.
[47] S.J. Annesley, S.T. Lay, S.W. De Piazza, O. Sanislav, E. Hammersley, C.Y. Allan, L. M. Francione, M.Q. Bui, Z.P. Chen, K.R.W. Ngoei, I.H.W. Ng, C.S. Palmer, P. Poronnik, C.A. McLean, A. Mackay-Sim, D.L. Pountney, P.R. Fisher, Immortalized Parkinson's disease lymphocytes have enhanced mitochondrial respiratory activity, Dis. Model. Mech. 9 (2016) 1295–1305, https://doi.org/10.1242/dmm.025684.